

Learning Decision Ensemble using a Graph Neural Network for Comorbidity Aware Chest Radiograph Screening

Arunava Chakravarty¹, Tandra Sarkar², Nirmalya Ghosh¹, Ramanathan Sethuraman³, Debdoot Sheet¹

Abstract—Chest radiographs are primarily employed for the screening of cardio, thoracic and pulmonary conditions. Machine learning based automated solutions are being developed to reduce the burden of routine screening on Radiologists, allowing them to focus on critical cases. While recent efforts demonstrate the use of ensemble of deep convolutional neural networks (CNN), they do not take disease comorbidity into consideration, thus lowering their screening performance. To address this issue, we propose a Graph Neural Network (GNN) based solution to obtain ensemble predictions which models the dependencies between different diseases. A comprehensive evaluation of the proposed method demonstrated its potential by improving the performance over standard ensembling technique across a wide range of ensemble constructions. The best performance was achieved using the GNN ensemble of DenseNet121 with an average AUC of 0.821 across thirteen disease comorbidities.

Index Terms—Chest X-ray screening, convolutional neural network, ensemble learning, GNN.

I. INTRODUCTION

Chest X-ray radiography (CXR) is a fast and inexpensive imaging modality which is commonly employed for the screening and diagnosis of cardio, thoracic and pulmonary pathologies. The shortage of Radiologists leads to unnecessary delays in the detection of diseases [1], which regresses early intervention. The routine nature of screening is inspiring the development of automated methods in order to prioritize the clinicians time and effort to the critical cases, as well as reduce the intra- and inter-observer variations in reporting.

The availability of large public datasets have led to the exploration of different Convolutional Neural Networks (CNNs) [2] for multi-label disease classification in CXR images. ResNet-50 [3] architecture was adapted in [4] and additional non-image data (viz. age, gender and the image view) were integrated to improve the classification. An attention guided CNN was explored in [5] where the disease specific regions of interest was estimated first to restrict the classification network’s inference to these regions only. Averaging the predictions from an ensemble of multiple CNN models has shown improved performance over single CNNs in [6] that employed an ensemble of 30 DenseNet [7] models, and in [8] that employed an ensemble of ResNet [3] with squeeze and excitation blocks by varying the model initialization conditions and the training dataset distribution.

*This work is supported through a research grant from Intel India Grand Challenge 2016 for Project MIRIAD.

¹ A. Chakravarty, N. Ghosh, D. Sheet are with the Indian Institute of Technology Kharagpur, India-721302 ({arunava, nirmalya, debdoot}@ee.iitkgp.ac.in)

² T. Sarkar is with Apollo Gleneagles Hospital, Kolkata, India

³ R. Sethuraman is with Intel Technology India Pvt. Ltd. Bangalore, India

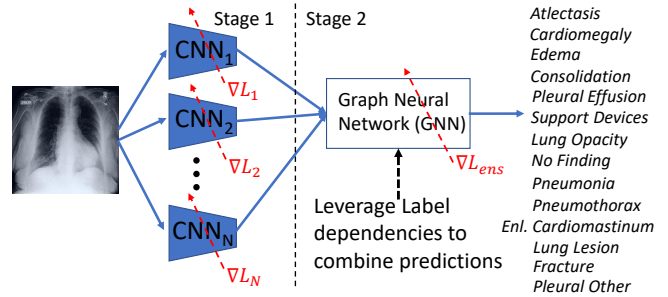


Fig. 1. Decision fusion of an ensemble of CNN models (Stage 1) using a comorbidity prior aware GNN (Stage 2).

Interestingly, chest diseases are pathologically correlated and this observation of joint or otherwise antagonistic appearance of a group of diseases is termed as comorbidity. The presence of a disease class statistically increases/decreases the probability of occurrence of other co-related classes (see Fig. 3). The existing methods have ignored these dependencies with an exception of an unpublished work [9] which employed a Recurrent Neural Network (RNN). However, this method requires the disease classes to be in a fixed order and only models the dependencies of a class with those preceding it. The construction of an ensemble of CNNs that combines the predictions by leveraging the comorbidity dependencies between the different diseases has not been explored so far.

In this work (Fig. 1), we explore a novel formulation using Graph Neural Networks (GNN) [10], [11] to combine the predictions of an ensemble of CNN models by leveraging the comorbidity statistics. The problem is modeled as a directed weighted graph where each disease class is represented by a vertex and the edge weights define the the degree of co-occurrence between each pair of vertices. A comprehensive evaluation of the method is performed by considering ensembles of different CNN architectures constructed by learning multiple network weights for each architecture and using different views of the image.

II. METHOD

The proposed framework depicted in Fig.1 is trained in two stages. In stage 1, an ensemble of CNN models is trained to obtain multiple prediction scores (one from each model in the ensemble) for each disease class. The model weights of the CNNs are frozen and the ensemble predictions are combined in stage 2. The task is modeled using a directed weighted graph to leverage the dependencies between the disease classes. Each disease is represented by a vertex in the graph and a GNN is trained to predict a label for each

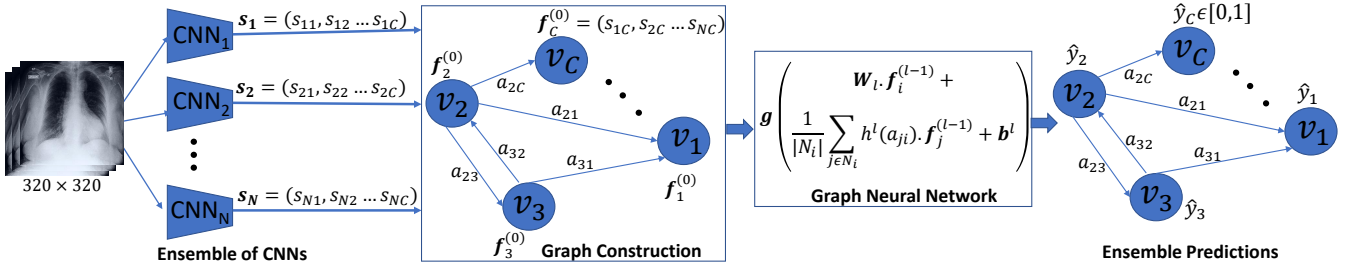


Fig. 2. Overview of the proposed Graph Neural Network Formulation to learn a comorbidity aware decision ensemble.

vertex which denotes the probability of occurrence of the corresponding disease. The details are discussed below.

Ensemble Construction: A standard CNN architecture is selected and its final layer is replaced by a fully connected (FC) layer comprising 14 neurons with sigmoid activations. It outputs a *multi-hot* encoding to detect the presence of one or more disease classes. The CNN is initialized with ImageNet [12] pre-trained weights while FC is randomly initialized. An ensemble for the CNN is constructed by training multiple network weights and employing different views of an image during prediction.

A Snapshot Ensembling (SE) [13] approach is employed during training to save multiple network weights for each CNN. The initial learning rate lr_{mx} is decayed to 0 over a cycle of batch updates using cosine annealing. Next, a warm restart is performed by re-initializing the learning rate to lr_{mx} to allow the network to escape a local minima and the training cycle is repeated multiple times, saving the network weights at the end of each cycle. The weights learned at the end of each training cycle acts as the initialization for the next one.

An ensemble of models is constructed by : i) training a separate CNN on each fold of a four-fold cross-validation on the training set; ii) using SE to obtain multiple network weights and selecting the top Q weights with the highest cross-validation performance for each fold and iii) employing a 5-crop of the input image (four corner and a central crop) during prediction to obtain a set of 5 predictions for each network weight. Thus, an ensemble of $N = 20 \cdot Q$ (4 folds \times Q weights \times 5 crops) network predictions is constructed.

In Fig. 2, the n^{th} prediction in the ensemble denoted by $s_n = (s_{n1}, s_{n2}, \dots, s_{nC}) \in \mathbb{R}^C$ is a *multi-hot* vector, where C is the total number of disease classes and each $s_{ni} \in [0, 1]$ is the probability of the input image to belong to the i^{th} class. **Graph Construction:** As depicted in Fig. 2, a graph $G(V, A)$ is constructed where $V = \{v_i | 1 \leq i \leq C, i \in \mathbb{Z}\}$ is a set of C vertices such that the vertex v_i corresponds to the i^{th} disease class. An input feature vector $f_i^{(0)} \in \mathbb{R}^N$ is constructed for each v_i by concatenating individual predictions from the N CNNs for the i^{th} class, ie., $f_i^{(0)} = (s_{1i}, s_{2i}, \dots, s_{Ni}) \in \mathbb{R}^N$.

Each element a_{ij} of the adjacency matrix $A \in [-1, 1]^{C \times C}$ is the edge weight between v_i, v_j and is a measure of the degree of co-occurrence between the two disease classes measured using the Cohen's κ metric [14]. κ is a more robust measure in comparison to percentage agreement as it takes

into account the probabilities of the two disease classes to co-occur by random chance. It is bounded in $[-1, 1]$ with values close to 1/-1 indicating a strong positive/negative correlation and 0 indicating independence between the two disease classes [14]. As a preprocessing step, the self loops in the graph are removed (by assigning $a_{ii} = 0$). Moreover, in order to reduce the computations in the GNN, A is pruned by only retaining the edges to the K neighbors for each node which have the maximum $|a_{ij}|$ values.

Graph Neural Network: The GNN is a deep network with L layers that accepts the graph adjacency matrix A and all vertex features $f_i^{(0)}$ as input to predict a 1-dimensional label $\hat{y}_i \in [0, 1]$ for each vertex v_i . Each layer $l \in [1, L]$ performs a Message Passing (MP) operation on the d_{l-1} dimensional feature representations $f_i^{(l-1)}$ from the previous $(l-1)^{th}$ layer to compute a d_l dimensional feature $f_i^{(l)}$ for each v_i . The output of the final L^{th} layer is the 1-dimensional prediction score, ie., $\hat{y}_i = f_i^{(L)}$. Mathematically, the MP operation is defined as

$$f_i^{(l)} = g \left(\mathbf{W}_l \cdot f_i^{(l-1)} + \frac{1}{|\mathcal{N}_i|} \sum_{j \in \mathcal{N}_i} h^l(a_{ji}) \cdot f_j^{(l-1)} + \mathbf{b}_l \right), \quad (1)$$

where $\mathbf{W}_l \in \mathbb{R}^{d_l \times d_{l-1}}$ and $\mathbf{b}_l \in \mathbb{R}^{d_l}$ are learnable weights of the l^{th} layer of the GNN. \mathcal{N}_i represents the set of immediate neighbors for v_i connected by direct edges. $g()$ is the activation function where $ReLU()$ is employed in all except the final layer where $Sigmoid()$ activation is used to obtain the class prediction scores and $h^l()$ is a fully connected network. The MP for each v_i comprises three operations: i) The node feature $f_i^{(l-1)}$ is transformed into a d_l dimensional vector by matrix multiplication with \mathbf{W}_l . ii) Next, the features $f_j^{(l-1)}$ from the immediate neighbors of v_i are aggregated into a d_l dimensional feature (details of the Aggregation Function is discussed below). iii) The transformed node and the aggregated neighborhood features are added with the bias \mathbf{b}_l and the activation function $g()$ is applied to obtain $f_i^{(l)}$.

Since, graphs (unlike images or N-D lattices) donot define a specific ordering among the neighbors, the GNNs employ a permutation invariant Aggregation Function. Traditionally, an average or max operation is employed [10] which leads to a loss of structural information as it treats each neighbor identically without considering the edge-weights. Hence, inspired from [11], we employ a *weighted* summation operation for aggregation. A weight matrix is learned for each

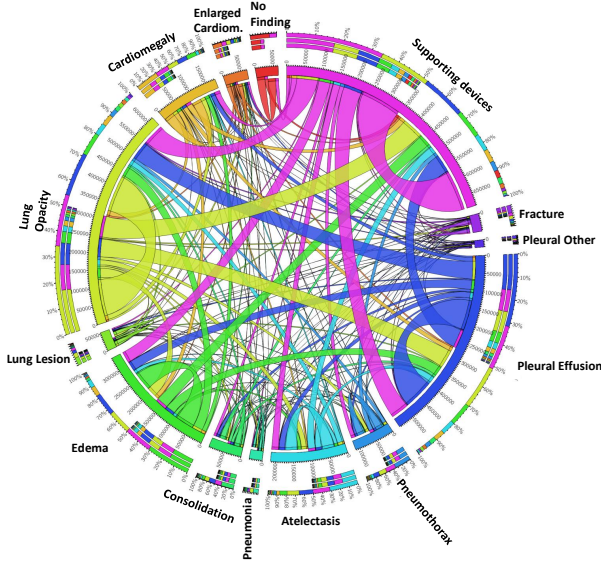


Fig. 3. Chord diagram representing the distribution of fourteen comorbid chest diseases in the CheXpert training dataset. The classes occupy an arc length along circumference proportional to its frequency. The thickness of the links connecting a pair of classes indicates their degree of co-occurrence.

feature $\mathbf{f}_j^{(l-1)}$ using a multi-layer perceptron h^l which takes the corresponding edge-weight a_{ji} as input. It comprises two fully connected layers. The first layer has $\lfloor \frac{d_l \times d_{l-1}}{2} \rfloor$ neurons with $ReLU()$ activation followed by the second layer whose output is reshaped to a $(d_l \times d_{l-1})$ weight matrix. $Tanh()$ operation is used in the final layer to allow negative values.

III. EXPERIMENTS

Dataset: The proposed method has been evaluated on the CheXpert dataset [6] which consists of 223,414 training and 234 test images with Ground Truth (GT) labels for 14 diseases. The GT for the training set is noisy and labeled as either present (1), absent (0) or uncertain (-1) as they were automatically obtained from free-text radiology reports. In our experiments, the uncertain labels were treated as the absence of the disease. The dependencies between the various classes is depicted in Fig. 3. GT for the test set did not have uncertain labels and obtained from the majority consensus opinion of 3 Radiologists [6]. There are no samples of the ‘‘Fracture’’ class in the test set.

Training: The *Binary cross-entropy loss* is used to train each CNN in stage 1 and the GNN in stage 2. The input 2D grayscale chest radiographs are pre-processed by resizing them to 320×320 and replicating to obtain a 3-channel input for the CNNs. The channels are normalized to match the statistics of the ImageNet [12] dataset. Data augmentation comprising random horizontal flips and random crops followed by resize operation are applied to the training images on-the-fly. The experiments were run on a server with $2 \times$ Intel Xeon 4110 CPU, 12×8 GB DDR4 RAM, $4 \times$ Nvidia GTX 1080Ti GPU with 11 GB RAM and Ubuntu 16.04 operating system. The models were implemented in

Python using the Pytorch 1.0 and Pytorch Geometric¹ library.

The CNN models in the ensemble were trained using SE for 7 cycles (each cycle is of 2 epochs with 10,647 batch updates per epoch, batch size of 16 and $lr_{mx} = 10^{-4}$) using the Adam optimizer [16] to select the top $Q = 2$ model weights with highest cross-validation performance.

The GNN was trained for 8 epochs, 22,341 batch updates per epoch with a batch size of 8 using Adam [16] optimizer, learning rate of 10^{-4} and a weight decay of 1×10^{-5} .

Result: A comprehensive evaluation of the proposed method is performed on ensembles constructed with identical CNN architecture but different network weights learned using SE on four folds of the training set and using five-crop views for each test image. The ResNet-18 [3], DenseNet-121 [7] and the Xception [15] architectures have been considered.

The hyperparameters for the GNN were empirically fixed through experimentation: (i) k neighbors considered for each vertex was fixed to 5 for ResNet, DenseNet and 9 for the Xception ensembles. (ii) Number of layers L was fixed to 5 for ResNet, 8 for DenseNet and 6 for Xception ensembles. (iii) For all the three ensembles, the input vertex features dimensionality $d_0 = 40$, the dimensionality d_1 of the output of 1st layer was fixed to 30 and the feature dimensionality was progressively increased across the layers as $d_l = \lfloor 1.3 \times d_{l-1} \rfloor, \forall 2 \leq l \leq L - 1$ for all ensembles, with $d_L = 1$ in the final L^{th} layer to obtain the class predictions.

The Area under the ROC curve (AUC) for each disease class in the test set is reported in Table 1². The baseline average ensembles used the same set of CNN models as employed in stage 1 of the proposed method but obtained the final ensemble decision by averaging the predictions of the individual CNN models instead of employing a GNN. Considering the average AUC values across all the thirteen disease classes reported in the last column of Table 1, we make the following observations. Both the GNN and the baseline ensemble models performed superior to the corresponding single model in terms of the average AUC values. Furthermore, *The proposed GNN based ensembles consistently outperformed the corresponding baseline ensembles with an improvement of $(\frac{0.820-0.775}{0.775} \times 100 =) 5.8\%$ for ResNet, $(\frac{0.821-0.782}{0.782} \times 100 =) 4.99\%$ for DenseNet and $(\frac{0.810-0.785}{0.785} \times 100 =) 3.19\%$ for the Xception architecture ensembles.* Among the three GNN ensembles, DenseNet performed the best (AUC=0.821) closely followed by ResNet (AUC=0.820) while the Xception ensemble had a marginally lower performance (AUC=0.810). A qualitative evaluation of the region where the DenseNet ensemble attended for classification was performed by treating the entire ensemble as a black box and employing the Randomized Input Sampling for Evaluation (RISE) [17] to compute the saliency maps. The saliency maps for the GNN based ensembles were in general found to be closer to the manual annotations by a Radiologist in comparison to the average baseline ensemble on a subset of test images (see Fig. 4 for few examples).

¹<https://pytorch-geometric.readthedocs.io/>

²Due to space limitations, the Sensitivity, Specificity metrics and ROC plots are available online at http://bit.do/Suppl_EMBC_GNN

TABLE I

AREA UNDER THE ROC CURVES (AUC) FOR THE CHEST X-RAY DISEASE CLASSIFICATION. THE AVERAGE AUC ACROSS THE THIRTEEN DISEASE CLASSES IS REPORTED IN THE LAST COLUMN. THE BEST PERFORMANCE OF EACH ARCHITECTURE IS INDICATED IN BOLD FOR EACH DISEASE. (S) DENOTES A SINGLE MODEL, (E) DENOTES ENSEMBLE BY AVERAGING PREDICTIONS AND (GNN) DENOTES THE PROPOSED ENSEMBLES COMBINED USING GNN.

	Atelectasis	Cardio-megaly	Edema	Consolid-ation	Pleural Effusion	Support Devices	Lung Opacity	Enlarged Cardiom.	No Finding	Pneum-onia	Pneumo-thorax	Lung Lesion	Pleural Other	Avg.
ResNet18 (S) [3]	0.721	0.735	0.916	0.893	0.931	0.904	0.910	0.462	0.857	0.622	0.729	0.189	0.893	0.751
ResNet18 (E)	0.756	0.787	0.909	0.907	0.938	0.943	0.927	0.488	0.886	0.733	0.839	0.017	0.944	0.775
ResNet18 (GNN)	0.773	0.821	0.906	0.870	0.937	0.936	0.926	0.615	0.894	0.502	0.850	0.657	0.983	0.820
DenseNet121(S) [7]	0.746	0.781	0.912	0.939	0.937	0.934	0.918	0.463	0.881	0.611	0.807	0.017	0.944	0.761
DenseNet121(E)	0.764	0.787	0.924	0.923	0.944	0.954	0.932	0.523	0.884	0.677	0.835	0.069	0.953	0.782
DenseNet121(GNN)	0.785	0.799	0.908	0.922	0.942	0.948	0.931	0.627	0.865	0.597	0.858	0.528	0.966	0.821
Xception(S) [15]	0.781	0.762	0.899	0.911	0.926	0.923	0.910	0.465	0.873	0.655	0.862	0.288	0.914	0.782
Xception(E)	0.772	0.788	0.916	0.907	0.940	0.948	0.928	0.475	0.878	0.679	0.863	0.150	0.966	0.785
Xception(GNN)	0.786	0.835	0.915	0.865	0.933	0.941	0.916	0.586	0.879	0.575	0.910	0.476	0.897	0.810

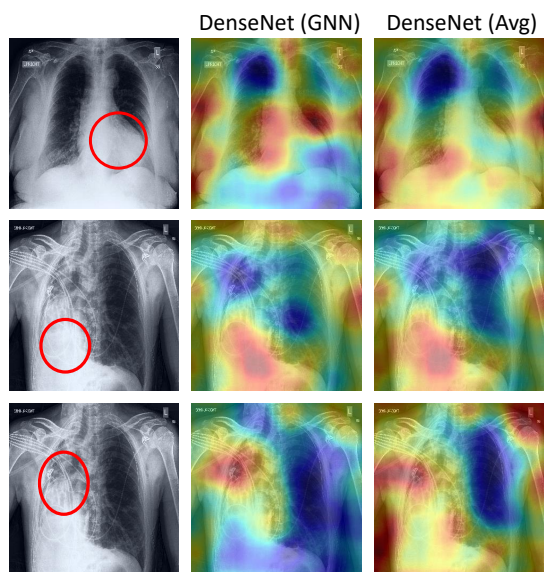


Fig. 4. RISE [17] based saliency map visualization for the proposed GNN (column 2) and baseline average ensembles (column 3) of DenseNet-121. The abnormal region is marked in RED by a Radiologist (column 1). Top row: Cardiomegaly; Middle row: Pleural Other; Bottom row: Lung Opacity. Middle and Bottom rows are comorbid diseases in the same CXR image.

IV. CONCLUSION

We explored a novel GNN based framework to obtain ensemble predictions by modeling the dependencies between different diseases in chest radiographs. A comprehensive evaluation of the proposed method demonstrated its potential by improving the performance over standard ensembling technique across a wide range of ensemble constructions. The best performance was achieved using the GNN ensemble of DenseNet121 with an average AUC of 0.821 across thirteen disease comorbidities. A systematic search over the hyperparameters of the GNN consisting of the number of layers, feature dimensionality in each layer, K nearest neighbors and the number of models used to construct the ensemble may further improve the performance. Since, the graph adjacency matrix was constructed using the noisy labels

in the training set that were obtained using automated NLP tools, a clinical validation/correction of these dependencies may be performed in the future.

REFERENCES

- [1] Abi Rimmer. Radiologist shortage leaves patient care at risk, warns royal college. *BMJ*, 359:j4683, 2017.
- [2] Xiaosong Wang, Yifan Peng, Le Lu, et al. Chestx-ray8: Hospital-scale chest x-ray database and benchmarks on weakly-supervised classification and localization of common thorax diseases. In *IEEE CVPR*, pages 2097–2106, 2017.
- [3] Kaiming He, Xiangyu Zhang, Shaoqing Ren, et al. Deep residual learning for image recognition. In *IEEE CVPR*, pages 770–778, 2016.
- [4] Ivo M Baltruschat, Hannes Nickisch, Michael Grass, Tobias Knopp, et al. Comparison of deep learning approaches for multi-label chest x-ray classification. *Scientific reports*, 9(1):6381, 2019.
- [5] Qingji Guan, Yaping Huang, Zhun Zhong, Zhedong Zheng, et al. Diagnose like a radiologist: Attention guided convolutional neural network for thorax disease classification. *arXiv:1801.09927*, 2018.
- [6] Jeremy Irvin, Pranav Rajpurkar, et al. Chexpert: A large chest radiograph dataset with uncertainty labels and expert comparison. *arXiv:1901.07031*, 2019.
- [7] Gao Huang, Zhuang Liu, Laurens Van Der Maaten, et al. Densely connected convolutional networks. In *IEEE CVPR*, pages 4700–4708, 2017.
- [8] Preetham Putha, Manoj Tadepalli, Bhargava Reddy, et al. Can artificial intelligence reliably report chest x-rays?: Radiologist validation of an algorithm trained on 2.3 million x-rays. *arXiv:1807.07455*, 2018.
- [9] Li Yao, Eric Poblenz, Dmitry Dagunts, Ben Covington, Devon Bernard, and Kevin Lyman. Learning to diagnose from scratch by exploiting dependencies among labels. *arXiv:1710.10501*, 2017.
- [10] William L. Hamilton, Zitao Ying, and Jure Leskovec. Inductive representation learning on large graphs. In *NeurIPS*, pages 1024–1034, 2017.
- [11] Martin Simonovsky and Nikos Komodakis. Dynamic edge-conditioned filters in convolutional neural networks on graphs. In *IEEE CVPR*, pages 29–38, 2017.
- [12] Olga Russakovsky, Jia Deng, Hao Su, et al. Imagenet large scale visual recognition challenge. *IJCV*, 115(3):211–252, 2015.
- [13] Gao Huang, Yixuan Li, Geoff Pleiss, Zhuang Liu, John E Hopcroft, and Kilian Q Weinberger. Snapshot ensembles: Train 1, get M for free. *ICLR*, 2017.
- [14] Mary L McHugh. Interrater reliability: the kappa statistic. *Biochemia medica*, 22(3):276–282, 2012.
- [15] François Chollet. Xception: Deep learning with depthwise separable convolutions. In *IEEE CVPR*, pages 1800–1807, 2017.
- [16] Diederik P. Kingma and Jimmy Ba. Adam: A method for stochastic optimization. In *ICLR*, 2015.
- [17] Vitali Petsiuk, Abir Das, and Kate Saenko. RISE: randomized input sampling for explanation of black-box models. pages 151–164, 2018.

SUPPLEMENTARY MATERIALS: LEARNING DECISION ENSEMBLE USING A GRAPH NEURAL NETWORK FOR COMORBIDITY AWARE CHEST RADIOGRAPH SCREENING

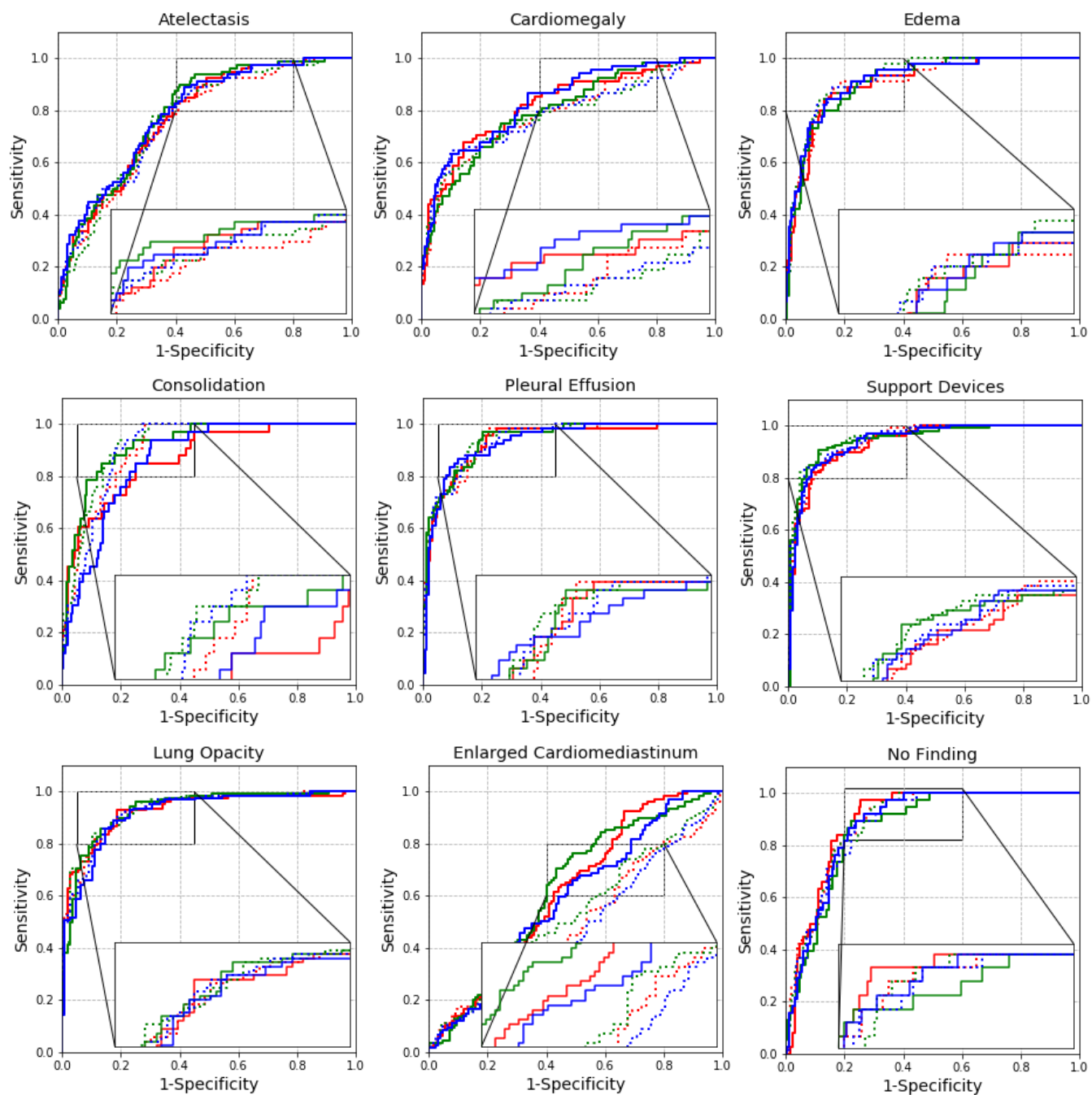


Fig. 5. The ROC plots for the nine disease classes. The performance of the proposed GNN ensemble constructed using ResNet is plotted in RED, DenseNet in GREEN and Xception in BLUE. The corresponding baseline average ensembles are plotted using dotted lines of the same color.

TABLE II
 SENSITIVITY (SENS.) AND SPECIFICITY (SPEC.) FOR THE CHEST X-RAY DISEASE CLASSIFICATION. THE OPERATING POINT ON THE ROC CURVE WAS SELECTED TO MAXIMIZE THE THE YOUDEN'S INDEX ($J = \text{SENS.} + \text{SPEC.} - 1$). (S) DENOTES A SINGLE MODEL, (E) DENOTES ENSEMBLE BY AVERAGING PREDICTIONS AND (G) DENOTES THE PROPOSED ENSEMBLES COMBINED USING GNN.

	Atelectasis		Cardiomegaly		Edema		Consolidation		Pleural Effusion		Support Devices		Lung Opacity		Enlarged Cardiom.		No Finding		Pneumonia		Pneumothorax		Lung Lesion		Pleural Other	
	Sens.	Spec.	Sens.	Spec.	Sens.	Spec.	Sens.	Spec.	Sens.	Spec.	Sens.	Spec.	Sens.	Spec.	Sens.	Spec.	Sens.	Spec.	Sens.	Spec.	Sens.	Spec.	Sens.	Spec.	Sens.	Spec.
ResNet18(S)	0.938	0.448	0.559	0.867	0.889	0.873	0.939	0.741	0.910	0.826	0.888	0.772	0.738	0.944	0.055	0.984	0.895	0.750	0.750	0.633	0.500	0.876	1.000	0.189	1.000	0.893
ResNet18(E)	0.825	0.591	0.588	0.916	0.911	0.815	1.000	0.716	0.985	0.778	0.850	0.898	0.881	0.833	0.174	0.896	0.947	0.714	0.750	0.743	0.875	0.673	1.000	0.017	1.000	0.944
ResNet18(G)	0.825	0.610	0.676	0.855	0.867	0.847	0.848	0.751	0.955	0.784	0.822	0.921	0.929	0.815	0.927	0.336	0.974	0.745	0.375	0.903	1.000	0.624	1.000	0.657	1.000	0.983
DenseNet121(S)	0.825	0.591	0.618	0.861	0.889	0.847	0.939	0.851	0.866	0.874	0.944	0.850	0.810	0.870	0.917	0.152	1.000	0.730	0.625	0.664	0.750	0.965	1.000	0.017	1.000	0.944
DenseNet121(E)	0.775	0.682	0.691	0.789	0.867	0.862	0.939	0.811	0.925	0.838	0.916	0.874	0.841	0.898	0.422	0.656	0.947	0.709	0.750	0.695	0.750	0.805	1.000	0.069	1.000	0.953
DenseNet121(G)	0.900	0.584	0.750	0.729	0.800	0.873	0.848	0.866	0.970	0.796	0.907	0.898	0.857	0.870	0.706	0.568	0.895	0.776	0.375	0.934	1.000	0.580	1.000	0.528	1.000	0.966
Xception(S)	0.800	0.688	0.662	0.849	0.911	0.820	1.000	0.701	0.746	0.952	0.850	0.843	0.825	0.870	0.193	0.856	0.921	0.745	0.750	0.602	0.750	0.854	1.000	0.288	1.000	0.914
Xception(E)	0.850	0.578	0.647	0.898	0.889	0.841	0.909	0.821	0.881	0.856	0.841	0.945	0.905	0.815	0.101	0.952	0.895	0.765	0.625	0.823	1.000	0.611	1.000	0.150	1.000	0.966
Xception(G)	0.888	0.571	0.632	0.898	0.844	0.862	0.939	0.697	0.836	0.910	0.850	0.906	0.889	0.824	0.661	0.512	0.921	0.735	0.250	0.960	1.000	0.730	1.000	0.476	1.000	0.897